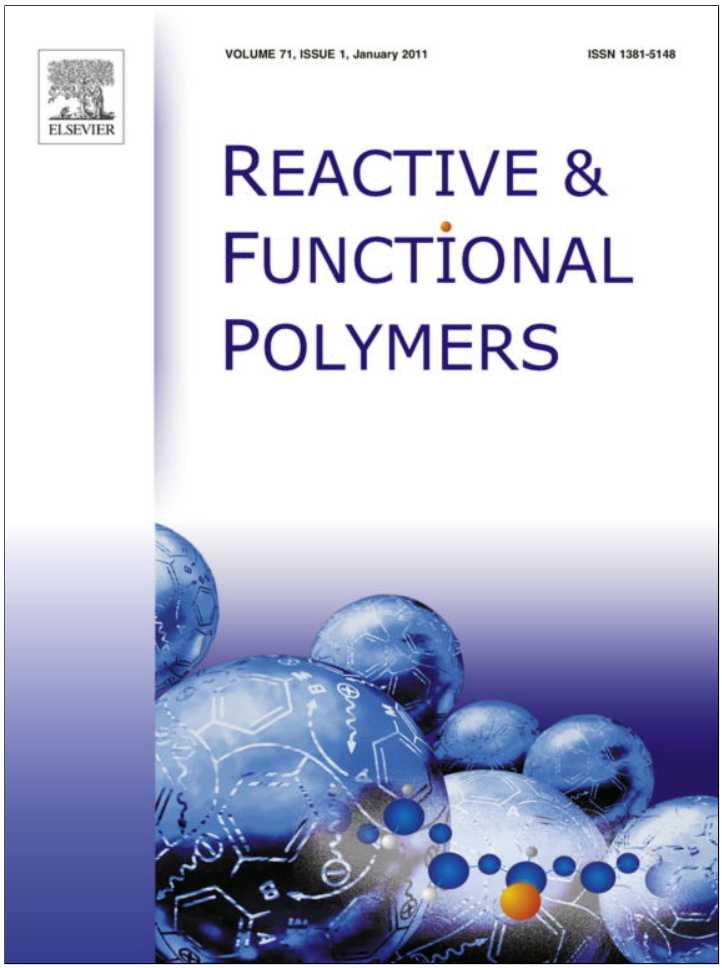

(This is a sample cover image for this issue. The actual cover is not yet available at this time.)

Reactive & Functional Polymers 72 (2012) 25–35

Contents lists available at SciVerse ScienceDirect

Reactive & Functional Polymers

journal homepage: www.elsevier.com/locate/react

Chemical oxidative polymerization of ethacridine

Budimir Marjanović [a], Ivan Juranić [b], Gordana Ćirić-Marjanović [c,*], Miloš Mojović [c], Igor Pašti [c], Aleksandra Janošević [d], Miroslava Trchová [e], Petr Holler [e], Jiří Horský [e]

[a] Centrohem, Vuka Karadžića bb, 22300 Stara Pazova, Serbia
[b] Faculty of Chemistry, University of Belgrade, Studentski Trg 12–16, 11158 Belgrade, Serbia
[c] Faculty of Physical Chemistry, University of Belgrade, Studentski Trg 12–16, 11158 Belgrade, Serbia
[d] Faculty of Farmacy, University of Belgrade, Vojvode Stepe 450, 11221 Belgrade, Serbia
[e] Institute of Macromolecular Chemistry, Academy of Sciences of the Czech Republic, 162 06 Prague 6, Czech Republic

ARTICLE INFO

Article history:
Received 10 May 2011
Received in revised form 8 September 2011
Accepted 8 October 2011
Available online 17 October 2011

Keywords:
Ethacridine
Electroactive oligomer
Functionalized oligoaminoacridine
Oxidative polymerization
Paramagnetism

ABSTRACT

Novel electroactive paramagnetic ethacridine oligomers were synthesized by the oxidation of ethacridine lactate with ammonium peroxydisulfate in acidic aqueous solution. The oxidative coupling of ethacridine was proved by gel permeation chromatography and MALDI-TOF mass spectrometry demonstrating the presence of oligomeric chains. Theoretical study of the mechanism of oxidation of ethacridine has been based on the semi-empirical quantum chemical computations of heat of formation and ionization energy of ethacridine, protonated ethacridine, generated reactive species and reaction intermediates, taking into account influence of pH and solvation effects. It was revealed that the prevalent ethacridine dimers are $N_{(C6)}$—C5 coupled. The influence of oxidant to monomer mole ratio on the molecular structure and the morphology of ethacridine oligomers has been studied by elemental analysis, FTIR, Raman, EPR and UV–Visible spectroscopies, MALDI-TOF mass spectrometry and scanning electron microscopy. Besides unoxidized monomeric units as prevalent, oligoethacridines contain the iminoquinonoid and newly formed fused phenazine units. The electroactivity of ethacridine oligomers was investigated by cyclic voltammetry.

1. Introduction

Polymers and oligomers of carbocyclic aryldiamines (phenylenediamines [1], aminodiphenylamines [2], diaminonaphthalenes [3], diaminoanthraquinones [4], benzidine [5], ring/*N*-substituted benzidines [6], and naphthidines [7]) and heterocyclic aryldiamines (diaminopyridines [8], diaminophenazines [9], diaminoacridines [10], and diaminocarbazoles [11]) have received increasing attention during the last two decades [12]. Molecular-weight distribution measurements revealed that the products of oxidative polymerization of aryldiamines are low- to high-molecular-weight oligomers rather than polymers. Aryldiamines are susceptible to oxidative polymerization *via* oxidation of one or both amino groups to give linear poly(aminoarylamines), polymers/oligomers containing phenazine units, and ladder polyphenazines. Poly(aryldiamines) have shown tunable electroactivity [13], high permselectivity to various electroactive species [14], unique electrochromism [15], linear sensitivity of the conductivity to moisture [16], controlled variation in the conductivity with temperature [17] and external electric field [18], high sensibilities of the polymer-modified electrodes to biosubstances at an extremely low concentration [19], good ability in detecting electroinactive anions [20], pronounced electrocatalytic properties [21], effective adsorption of heavy-metal ions [22], strong adhesion to metals [23], anticorrosion ability [24], and high capacitance [25].

Ethacridine lactate (2-ethoxy-6,9-diaminoacridine lactate), is well-known diaminoacridine antiseptic with the trade name Rivanol (Scheme 1) [26]. As in the case of most polymers and oligomers of aryldiamines, which have been prepared mainly by electrochemical polymerization [12], there is one report regarding electropolymerization of ethacridine by potentiostatic and cyclic voltammetric methods [27], however, without any structural characterization of poly(ethacridine) film at Pt electrode. Glucose oxidase was simultaneously incorporated into the matrixes of thin poly(ethacridine), which was developed to fabricate a glucose sensor which exhibited good stability and fast amperometric response to glucose [27]. To our knowledge there is no report relating to the chemical oxidative polymerization/oligomerization of ethacridine.

Objectives of the present work are the oxidation of ethacridine lactate with ammonium peroxydisulfate (APS) in aqueous solution, characterization of oxidation products by a variety of techniques, and elucidation of the polymerization mechanism using the semi-empirical AM1, PM3 and RM1 quantum chemical computational methods. Special attention has been paid to the study of the influence of oxidant/monomer mole ratio on physico-chemical

* Corresponding author. Tel.: +381 11 3336623; fax: +381 11 2187133.
E-mail address: gordana@ffh.bg.ac.rs (G. Ćirić-Marjanović).

1381-5148/$ - see front matter © 2011 Elsevier Ltd. All rights reserved.
doi:10.1016/j.reactfunctpolym.2011.10.002

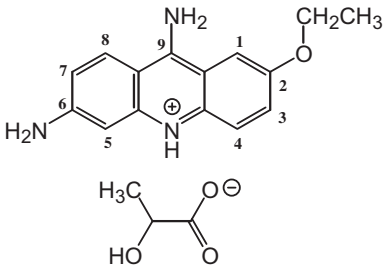

Scheme 1. Ethacridine lactate.

properties of oxidation products. The main structural features of ethacridine oligomers, revealed by FTIR, Raman, EPR, and UV–Visible spectroscopies, are correlated with the molecular structure of computationally predicted dominant ethacridine dimers.

2. Experimental

2.1. Materials

Ethacridine lactate-1-hydrate (extra pure, 99.9%, Centrohem, Serbia), APS (p.a., ⩾99%, Centrohem, Serbia), hydrochloric acid (0.1 M standard solution, Centrohem, Serbia), sulfuric acid (p.a., 96%, Centrohem, Serbia), and dimethyl sulfoxide (DMSO) (p.a., 99.9%, Centrohem, Serbia) were used as received.

2.2. Oxidation of ethacridine lactate

The oxidation of ethacridine lactate has been carried out in aqueous solution with APS at oxidant-to-monomer mole ratios 1.25 and 2.5. Obtained oxidation products are labeled in the following text as Oligoethacridine-1 and Oligoethacridine-2, respectively. The oxidant solution containing 2.85 or 5.70 g APS dissolved in 20 ml of distilled water was poured into the monomer solution containing 3.61 g of ethacridine lactate-1-hydrate dissolved in 250 ml of 0.1 M HCl, and the reaction mixture was left for 48 h with stirring, at 20 °C. The dark brown precipitated oxidation products were collected on a filter, rinsed with 0.01 M HCl, and dried in vacuum at 60 °C for 3 h.

2.3. Characterization of precipitated oxidation products

Molecular weights were assessed with a GPC/SEC apparatus using a 8 × 500 mm Labio GM 1000 column operating with *N*-methyl-2-pyrrolidone and calibrated by polystyrene standards, with a spectrophotometric detection at the wavelength of 546 nm. The sample was dissolved in *N*-methyl-2-pyrrolidone containing 0.025 g cm^{-3} triethanolamine for deprotonation and 0.005 g cm^{-3} lithium bromide to prevent aggregation. Flow rate was 1 ml min^{-1}. MALDI-TOF MS spectra were acquired with a Biflex III mass spectrometer (Bruker Daltonics) equipped with a 337 nm N2 laser using delayed extraction and either linear or reflectron measuring mode. No ionization agent was used. For matrixless measurements, the oligoethacridine was either directly deposited on the ground-steel target plate or 1 μL of 1% oligoethacridine solution (10 mg/mL) in DMSO was deposited and let to dry. If matrix was used, oligoethacridine solution was mixed with DMSO solution of dithranol (anthracene-1,8,9-triol; 20 mg/mL) in the volume ratio 1:5 prior to deposition. The external calibration on poly(ethylene glycol) was used. The electrical conductivity of oligoethacridine powder compressed between stainless steel pistons, within an isolating hard-plastic die, was measured at room temperature by means of an ac bridge (Waynne Kerr Universal Bridge B 224), working at fixed frequency of 1.0 kHz. During the measurement, the pressure was kept constant at 124 MPa. The scanning electron microscope JEOL JSM 6460 LV has been used to characterize the morphology of the oligoethacridines. Powdered material was deposited on an adhesive tape fixed to specimen tabs and then coated by ion sputtered gold using the BAL-TEC SCD 005 Sputter Coater prior to SEM measurements. Elemental analysis (C, H, N, S, Cl) was performed using the Perkin Elmer CHNS/O Analyzer 2400. Infrared spectra of the powdered samples dispersed in the KBr pellets were recorded in the range 400–4000 cm^{-1} at 64 scans per spectrum at 2 cm^{-1} resolution using the Thermo Nicolet NEXUS 870 FTIR spectrometer with the DTGS TEC detector. The spectra were corrected for the presence of carbon dioxide and humidity in the optical path. Raman spectra of oligoethacridines, excited with a diode-pumped solid state 532 nm laser, were collected on the Thermo Scientific DXR Raman microscope, equipped with a research optical microscope and a CCD detector. The laser beam was focused on the sample using objective magnification × 50. The powdered sample was placed on an *X*–*Y* motorized sample stage. The scattered light was analyzed by a spectrograph with grating 1800 lines mm^{-1}. Laser power was kept at 0.1 mW on the oligoethacridine sample in order to avoid its degradation. The correction of fluorescence was automatically done for oligoethacridine samples during the measurements. Raman spectrum of ethacridine lactate was collected on the Renishaw inVia Reflex Raman microscope by using a He–Ne 633 nm laser. A research-grade Leica DM LM microscope with objective magnification × 50 was used to focus the laser beam on the sample placed on an *X*–*Y* motorized sample stage. The scattered light was analyzed by the spectrograph with a holographic grating (1800 lines mm^{-1}). The Peltier-cooled CCD detector (576 × 384 pixels) registered the dispersed light. UV–Vis absorption spectra of the ethacridine lactate and oligoethacridine samples dissolved in DMSO (0.01 g dm^{-3}) were recorded using BECMAN DU–600 spectrophotometer. The EPR spectra of solid-state samples were obtained at room temperature using the Varian E104-A EPR spectrometer operating at X-band (9.3 GHz), using the following settings: 1 G modulation amplitude, 100 kHz modulation frequency, and 10 mW microwave power. Spectra were recorded and analyzed using EW software (Scientific Software). Cyclic voltammetry measurements were conducted at room temperature using the Gamry PCI4/750 potentiostat (Gamry Instruments, USA) controlled by Gamry Framework v4.35. Measurements were performed in a standard three-electrode electrochemical cell using glassy carbon (GC) electrode with geometrical surface area of 0.196 cm^2 as a working electrode and a saturated calomel electrode (SCE) as a reference electrode. As a counter electrode, large surface platinum plate was used. The oxidation products of ethacridine lactate were dissolved at a concentration of 2.5 g dm^{-3} in DMSO solution of H_2SO_4 (0.2 M), and this solution was studied by cyclic voltammetry. Prior to, and during each experiment, the solutions were purged with high purity nitrogen gas (5 N, Messer).

2.4. Theory: computational methods

Semiempirical AM1 and PM3 methods [28] (included in the molecular orbital program [29] MOPAC 97, a part of the Chem3D Pro 5.0 package, CambridgeSoft Corporation), as well as the RM1 method [30] (improved/reparameterized version of the AM1, included in the MOPAC 2009) have been used to obtain the bond lengths, Mulliken charges, and heat of formation (ΔH_f) of individual species. The AM1 method was proved to be accurate enough to has useful predictive power, and fast enough to allow the processing of large molecules such as aromatic amine oligomers and their intermediates [2a,31]. Solvation effects were taken into account using the conductor-like screening model (COSMO) to approximate the effect of water surrounding the molecule [32]. Conformational analysis of all intermediates is done. The steric energy was minimized by using the MM2 molecular mechanics force-field method [33]. Input files for the semiempirical quantum chem-

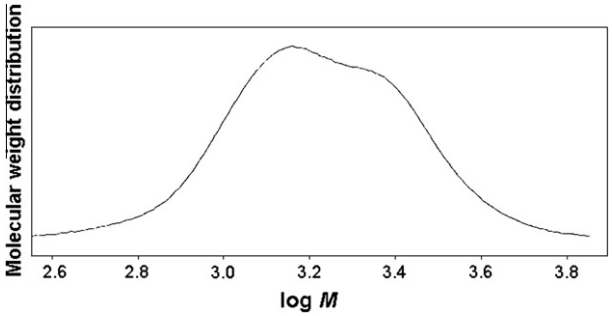

Fig. 1. Molecular weight distribution of Oligoethacridine-2, determined by GPC in *N*-methyl-2-pyrrolidone.

ical computations of all intermediates were the most stable conformers of investigated molecular structures. Geometry optimization was performed by the Eigenvector following procedure [34,35]. The Restricted Hartree–Fock method has been used.

3. Results and discussion

3.1. Molecular weights

The oxidation products of ethacridine lactate are low-molecular-weight oligomers, as proved by GPC (Fig. 1) and MALDI-TOF MS (Fig. 2). Oligoethacridine-1 and Oligoethacridine-2 samples show bimodal molecular-weight distribution with peak molecular weights M_{p1} = 1680 and 1450, and M_{p2} = 2750 and 2370, weight-average molecular weight M_w = 1980 and 1930, number-average molecular weight M_n = 1630 and 1560, and polydispersity M_w/M_n = 1.22 and 1.24, respectively. Since the polystyrene-based calibration is used, only apparent molecular weights are obtained by GPC, the error may be up to 100%. Because both M_w and M_n are affected, the errors partially compensate in the index of polydispersity; nevertheless the error in M_w/M_n still can achieve 30% [36]. Even higher errors may occur for oligomers for several reasons. The above estimates are based on the Mark–Houwink equation, describing the dependence of the intrinsic viscosity on molecular weight, and on the "universal calibration" concept, which both can fail for oligomers [37]. Therefore, MALDI-TOF MS analysis of oligoethacridines has also been performed. MALDI-TOF MS is a method suitable for low-molecular-weight polymers and oligomers [38]; however, reliable average molecular weight can be obtained only for samples with a narrow distribution of molecular weight, $M_w/M_n < 1.3$ [39]. MALDI-TOF mass spectrum of Oligoethacridine-1 obtained in linear measuring mode with dithranol as a matrix is given in Fig. 2A. Virtually the same spectrum was obtained for Oligoethacridine-2. The spectra cannot be used for calculation of usable average molecular weights even though the value of M_w/M_n obtained from GPC was low enough. The spectra consist of a series of peak

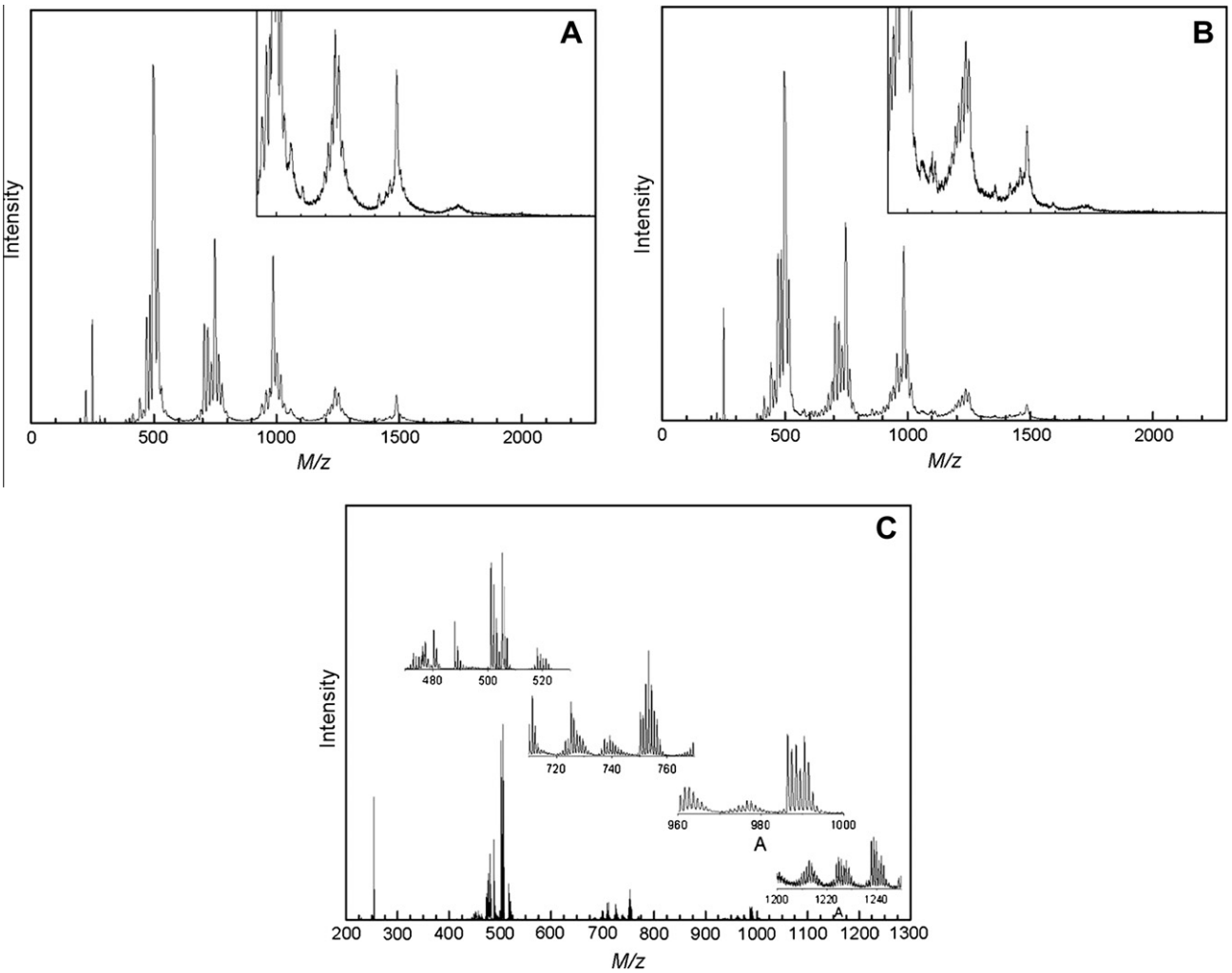

Fig. 2. MALDI-TOF mass spectrum of Oligoethacridine-1 (A) obtained in a linear mode by dry droplet method with dithranol as a matrix; the higher molecular weight region is expanded in the inset, (B) obtained in a linear mode by dry droplet method without a matrix; the higher molecular weight region is expanded in the inset, (C) obtained in a reflectron mode after direct deposition of Oligoethacridine-1 on the target plate; the expanded parts of peak clusters are inserted in the figure.

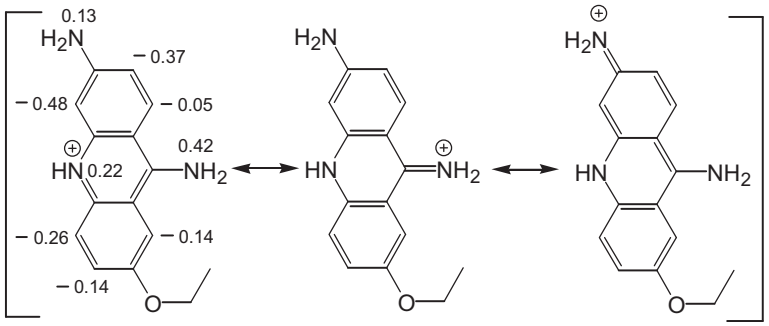

Scheme 2. Resonance canonical forms of protonated ethacridine. Charge distribution of protonated ethacridine in aqueous solution, calculated by the PM3/COSMO method, is shown.

clusters separated by roughly 250 Da, which is consistent with ethacridine oligomerization; the presence of oligomeric species from dimers up to hexamers is clearly evidenced. However, the strongest signal corresponds to the dimer and the intensity of peaks strongly decreases with molecular weight and is almost negligible in the region of maxima on molecular weight distributions obtained from GPC. The difference can be also caused by properties of MALDI-TOF MS: (i) The MS signal is proportional to the number of detected ions whereas molecular weight distribution gives the mass fraction; (ii) the MALDI-TOF MS response depends generally on M/z value; (iii) Possible fragmentation during desorption and ionization is frequently invoked while interpreting complicated MALDI-TOF mass spectra. Fragmentation would of course decrease observed molecular weight. The fact that a cluster of peaks rather than one peak corresponds to one "polymerization degree" is in favor of fragmentation. On the other hand, the increase in "fragmentation" was observed when the experiments were repeated without matrix, which should have protective effect, see Fig. 2B. Another possibility

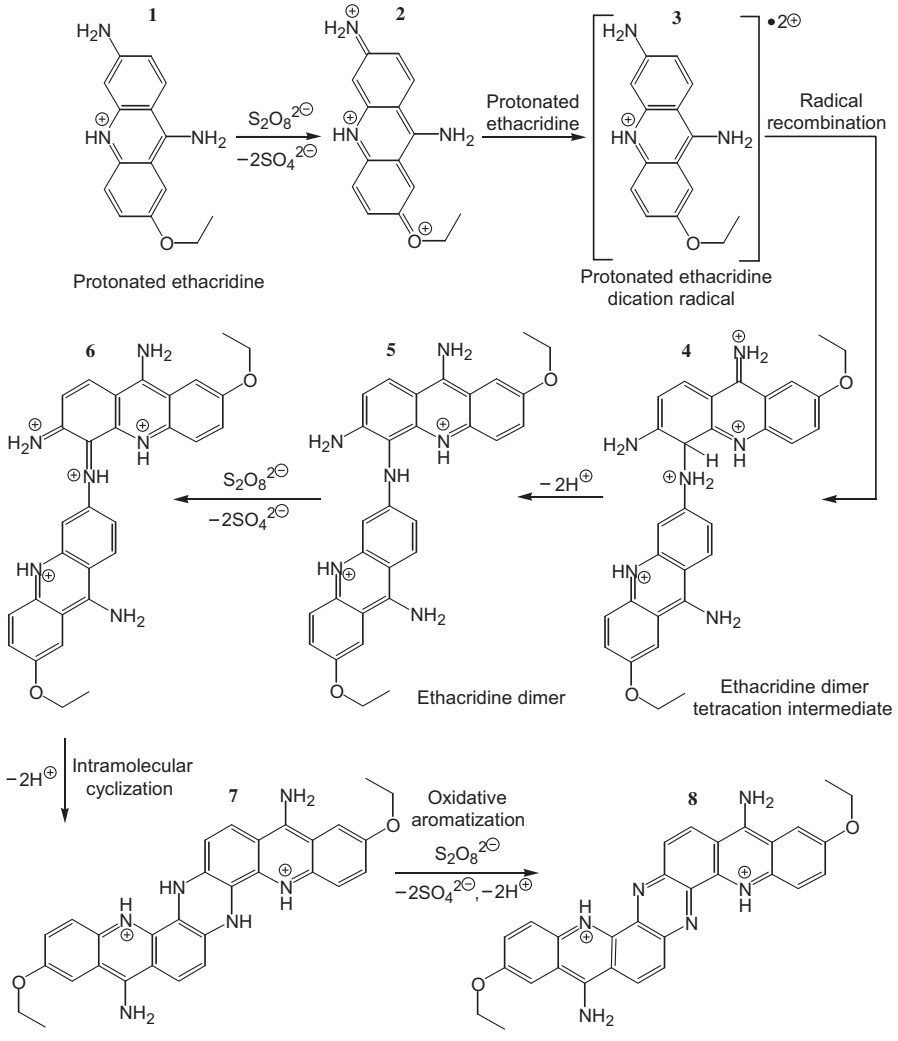

Scheme 3. Oxidative dimerization of protonated ethacridine with peroxydisulfate.

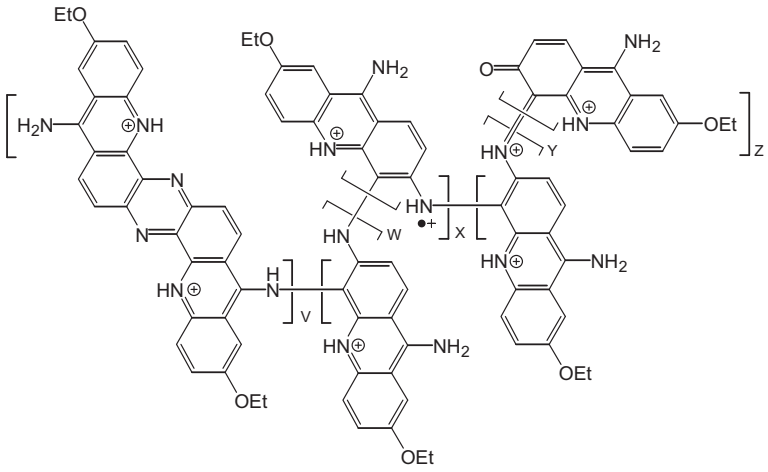

Scheme 4. Molecular structure of oligoethacridines.

which has to be considered is number of charges (z) of observed ions. The separation of peak clusters by values corresponding roughly to the molecular weight of the monomer already indicates $z = 1$. Unequivocal evidence is found in the spectrum measured in the reflectron mode (Fig. 2C), which has higher resolution but lower sensitivity. No peaks are observable above $M = 1250$ but observable peaks are well resolved. The separation of adjacent isotopic peaks by 1 Da proves $z = 1$. Further, positions of monoisotopic peaks are not compatible with the additional charges of ethacridine oligomers being compensated by anions whether lactate, sulfate or chloride; rather, excess charges seem to be eliminated by loss of protons. That may explain why longer oligomers seem to be underrepresented in the spectra. A longer ethacridine oligomer contains more charges and has to lose more protons in order to achieve $z = 1$ and thus smaller fraction of single-charged ions may be expected to be produced than for a shorter oligomer. Precision of molecular weight in the reflectron mode is so high that assignment of peaks to the structures given in Schemes 3 and 4 (after elimination of excess protons) can be attempted. However, such assignment was successful only for the monomer (structure 1, $M/z = 254$), dimers (structure **5**, $M/z = 501$ and structure **8**, $M/z = 505$) and a trimer with $v = 1$ and $w = 1$ ($M/z = 752$). Assignments of all other peaks failed, at least for the time being.

3.2. Conductivity and morphology

Oligoethacridines are nonconducting ($\sigma = 6.4 \times 10^{-9}$ S cm^{-1} and 6.5×10^{-9} S cm^{-1} for Oligoethacridine-1 and Oligoethacridine-2, respectively). They have fragmental and submicro/microlayered morphology, as revealed by SEM (Fig. 3).

3.3. Computational study of the oxidation of ethacridine with peroxydisulfate

The classical structural formula of ethacridine lactate is misleading, representing this heterocyclic aromatic compound exclu-

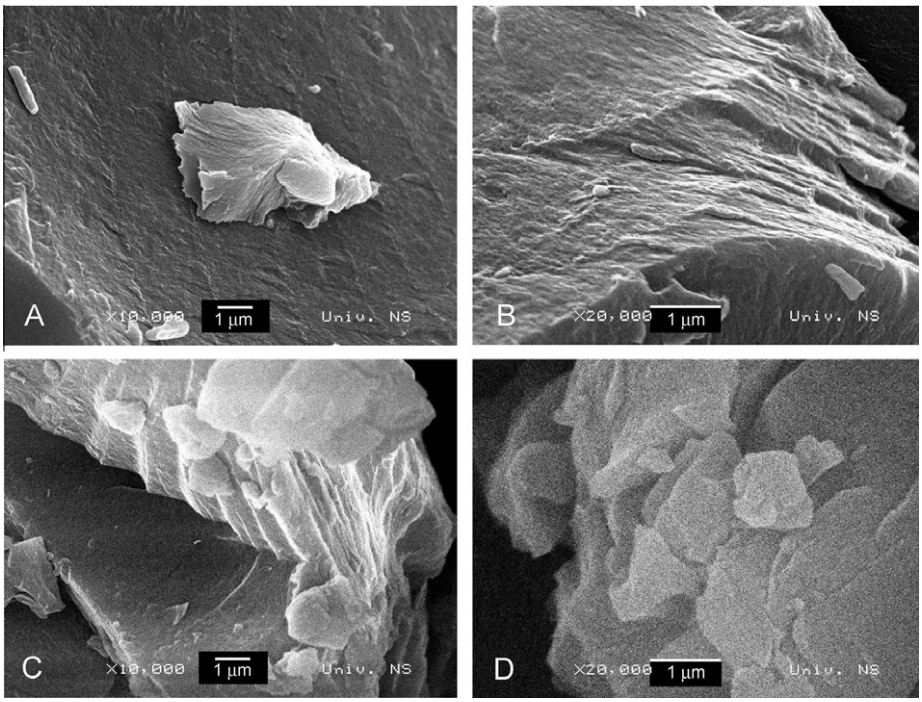

Fig. 3. SEM images of Oligoethacridine-1 (A, B) and Oligoethacridine-2 (C, D).

Table 1
Heat of formation of ethacridine dimer tetracation intermediates, ΔH_f(di-E^{4+}), generated by various coupling reactions of dication radicals of protonated ethacridine ($E^{\bullet 2+}$), computed by RM1/COSMO method.

Coupling mode $E^{\bullet 2+}$+$E^{\bullet 2+}$	ΔH_f ([di-E]$^{4+}$) kcal mol^{-1}	Coupling mode $E^{\bullet 2+} + E^{\bullet 2+}$	ΔH_f ([di-E]$^{4+}$) kcal mol^{-1}	Coupling mode $E^{\bullet 2+} + E^{\bullet 2+}$	ΔH_f ([di-E]$^{4+}$) kcal mol^{-1}
$N_{(C9)}$—$N_{(C9)}$	509.8	$N_{(C6)}$—$N_{(A)}$	472.2	$N_{(A)}$—C7	441.4
$N_{(C9)}$—$N_{(C6)}$	479.6	$N_{(C6)}$—C4	422.1	C4—C4	436.9
$N_{(C9)}$—$N_{(A)}$	484.0	$N_{(C6)}$—C5	407.5	C4—C5	418.9
$N_{(C9)}$—C4	449.2	$N_{(C6)}$—C7	409.1	C4—C7	434.4
$N_{(C9)}$—C5	441.0	$N_{(A)}$—$N_{(A)}$	495.3	C5—C5	416.6
$N_{(C9)}$—C7	428.3	$N_{(A)}$—C4	447.0	C5—C7	410.3
$N_{(C6)}$—$N_{(C6)}$	446.7	$N_{(A)}$—C5	439.7	C7—C7	408.0

sively as aryldiamine (Scheme 1). In fact, protonated ethacridine has a partial iminopyridonoid as well as iminoquinonoid character (Scheme 2). This was confirmed by the PM3/COSMO-computed charge distribution of protonated ethacridine (Scheme 2), showing substantial delocalization of positive charge over three nitrogen atoms (acridine ring nitrogen as well as both amino nitrogen atoms).

It has recently been shown that arylnitrenium cations are formed in the initiation phase of the oxidation of primary arylamines with $S_2O_8^{2-}$ in an aqueous solution, whenever the formation of *para*/*ortho*-iminoquinonoid intermediate and/or product is not possible [2,6,40–42]. Two-electron oxidation of protonated ethacridine (**1**) with $S_2O_8^{2-}$ leads to the formation of iminoquinonoid intermediate (**2**). Based on the modified Epiotis constraint $|E_{HOMO\ (D)} - E_{LUMO\ (A)}| < |E_{HOMO\ (A)} - E_{LUMO\ (D)}|$ [D represents an electron donor (reductant) and A stands for an electron acceptor (oxidant)], our computations have proved that protonated ethacridine can be easily oxidized with iminoquinonoid intermediate (single electron transfer reaction), thus leading to the generation of dication radicals of protonated ethacridine (**3**, Scheme 3).

The generated dication radicals of protonated ethacridine ($E^{\bullet 2+}$) instantaneously undergo radical recombination reaction, leading to the formation of dimeric tetracation intermediates (**4**), further being transformed to ethacridine dimers (**5**) by releasing protons (Scheme 3). Spin delocalization of $E^{\bullet 2+}$, represented by its resonance hybrid, indicates that nitrogen atoms of both amino groups ($N_{(C6)}$ and $N_{(C9)}$) as well as nitrogen ($N_{(A)}$) and carbon atoms (C4,C5,C7) of acridine ring are reactive sites for radical coupling. According to the Hammond postulate [43], the radical recombination reaction of $E^{\bullet 2+}$ is not governed by the stability of the final dimeric products but is governed by the stability of ethacridine dimer tetracation intermediates ([di-E]$^{4+}$), resembling structurally the transition state, as nearest to it on the reaction path. Based on RM1/COSMO computations of the heat of formation (ΔH_f) of [di-E]$^{4+}$ (Table 1), it has been concluded that $N_{(C6)}$–C5 is the dominant coupling mode for ethacridine (**5**, Scheme 3). The coupling reactions C7–C7 and $N_{(C6)}$–C7 of $E^{\bullet 2+}$ also occur in some extent.

Prevalent $N_{(C6)}$–C5 coupled ethacridine dimer (**5**, [di-E]$^{2+}$) can be further oxidized to various products. Two-electron oxidation of [di-E]$^{2+}$, followed by intramolecular cyclization, lead to the formation of dihydrophenazine-like structures (**7**, Scheme 3) which can be easily oxidized further to phenazine-like structures (**8**, Scheme 3). Our RM1/COSMO computational results suggest that intramolecular cyclization is thermodynamically favorable, because it leads to the formation of dihydrophenazine-containing dimer [ΔH_f = 176.7 kcal mol^{-1} (**7**, Scheme 3)] which is more stable than corresponding non-cyclized ortho-iminoquinonoid dimer [ΔH_f = 222.1 kcal mol^{-1} (**6**, Scheme 3)], both compared species bearing the same oxidation and protonation state. It seems that formation of ladder segments during the course of oxidative polymerization of ethacridines, characteristic of a number of aromatic diamine polymers growth mechanisms [12], could be expected.

3.4. Molecular structure of oligoethacridines

3.4.1. Elemental analysis

The elemental composition of oligoethacridines (Table 2) indicates the presence of sulfur and chlorine due to the incorporation of sulfate/hydrogen sulfate and chloride anions as counter ions of positively charged oligoethacridine chain. The lower C/N mole ratio in synthesized oligoethacridines (~5.25) compared with that of ethacridine lactate (6.00) is most probably due to the significantly decreased content of lactate anions in oligoethacridines in comparison with ethacridine lactate, because sulfuric and hydrochloric acid, as strong mineral acids (pK_a < 0), expel lactic acid as a weak carboxylic acid (pK_a = 3.86) from its salts (ethacridine and oligoethacridine lactate).

3.4.2. FTIR spectroscopy

The observed bands in the FTIR spectra of ethacridine lactate and oligoethacridine samples (Figs. 4 and 5) are summarized in Tables 3 and 4 with their tentative assignments. The FTIR spectrum of ethacridine lactate (Fig. 4) exhibits the bands at 3421 and

Table 2
Elemental composition of Oligoethacridine-1 and Oligoethacridine-2, determined by elemental analysis (C, H, N, S and Cl) and by difference (O), and calculated elemental composition of monomer ethacridine lactate.

Sample	Content (wt%)					
	C	H	N	O	S	Cl
Ethacridine lactate	62.96	6.16	12.24	18.64	–	–
Oligoethacridine-1	52.52	5.15	11.73	24.91	4.21	1.48
Oligoethacridine-2	52.50	4.64	11.64	26.38	3.84	1.00

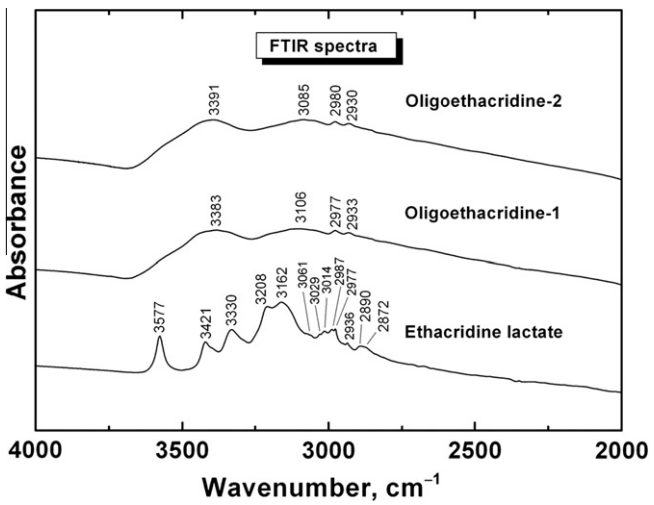

Fig. 4. FTIR spectra of ethacridine lactate and oligoethacridine samples in the wavenumber region 4000–2000 cm^{-1}.

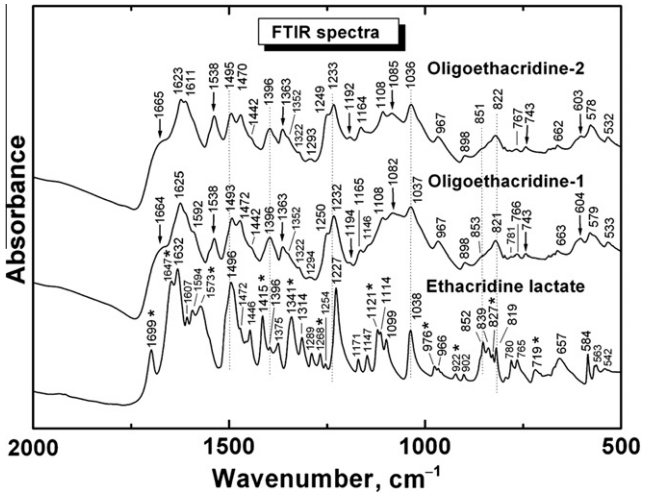

Fig. 5. FTIR spectra of ethacridine lactate and oligoethacridine samples in the wavenumber region 2000–500 cm^{-1}. The new bands which appeared in the spectra of oligomers in comparison with the monomer spectrum are marked with an arrow; the bands of monomer which are absent in the spectra of oligomers are marked with an asterisk.

3330 cm^{-1} which are assigned to the asymmetric, ν_{as}(N–H), and symmetric, ν_s(N–H), free N–H stretching vibrations of primary aromatic amino groups. [2a,9,44–46]. The disappearance of these bands in the FTIR spectra of oligomers (Fig. 4, Table 3), and appearance of a new broad band in the spectra of Oligoethacridine-1 and Oligoethacridine-2 centered at 3383 and 3391 cm^{-1}, respectively, attributed to the N–H stretching vibrations of secondary amino groups and imino groups [45], indicates the transformation of primary amino groups of monomer into the secondary amino and/or imino groups during the oxidation reaction. The very broad shape of the later band is connected with a strong hydrogen bonding, which involves different types of intra- and intermolecular hydrogen-bonded N–H stretching vibrations in oligomers (*e.g.*, N–H···N, $NH^{+}\cdots$N, =NH···N).

The band observed at 1647 cm^{-1} in the spectrum of ethacridine lactate (Fig. 5) may be attributed to the C=N stretching vibration, ν(C=N), with possible contribution of primary amino group deformation mode, $\delta(NH_2)$, with H-bonding (Table 4). This band disappears in the spectra of oligomers, while a new band (rather a shoulder) appears at ~1664 cm^{-1}. The latter band is attributable to the mixed ν(C=N) and ν(C=O) vibrations, where C=O group is present in quinonoid-like structures that could be formed by the hydrolysis of imine C=N bonds in oligomers (Scheme 4).

Among the most notable FTIR spectral differences between oligoethacridines and ethacridine lactate monomer is the appearance of new bands at 1538 and 1363 cm^{-1} in the spectra of oligomers, which are not present in the spectrum of monomer. These bands are indicative for the formation of a new aromatic system in oligomeric chains, and are attributable to the ring-stretching vibrations of phenazine-like structural units formed by an intramolecular cyclization process (6 → 7 → 8 in Scheme 3) [9].

The ethoxy group did not participate in the polymerization process, as revealed by the presence of characteristic bands of this group [44] in the spectra of oligoethacridines at wavenumbers ~2933, ~1233, ~1108 and 767 cm^{-1}, close to those in the spectrum of monomer at 2936, 1227, 1114, and 765 cm^{-1}, respectively (Figs. 4 and 5, Tables 3 and 4).

In the spectral region of the C—N stretching vibrations, ν(C—N), of aromatic amines (~1360–1250 cm^{-1}), the monomer spectrum exhibits the bands at 1289 and 1268 cm^{-1} (Fig. 5), both corresponding to the ν(C—N) vibrations of primary aromatic amines [2a,9,44,45]. The appearance of two distinct bands could be explained by the different nature of the aromatic rings to which the amino groups are attached, one NH_2 group being bonded to the fused benzene ring (C6 position), and second one to the fused pyridine ring (C9 position). Our semiempirical AM1/COSMO quantum chemical computations have shown that the C9—N bond is shorter (0.1329 nm) than the C6—N bond (0.1364 nm), indicating thus that the band at 1289 cm^{-1} corresponds to stretching vibration of the C9—N bond, while the band at 1268 cm^{-1} corresponds to stretching vibration of the C6—N bond. In the FTIR spectra of oligoethacridines the band at 1268 cm^{-1} completely disappeared, but the existence of a weak band at 1293 cm^{-1} indicates the presence of unoxidized NH_2 group bonded to fused pyridine ring in oligomeric chains. This spectroscopic finding is in excellent agreement with computational predictions of the mechanism of ethacridine oligomerization via the oxidative coupling of amino group bonded to C6 position of the acridine ring. Instead of monomer bands at 1341 and 1314 cm^{-1}, assigned to ν(C—N) vibrations mixed with the acridine ring-stretching vibrations [44,47], the spectra of oligomers exhibit new shoulder at 1352 cm^{-1} and a weak band at 1322 cm^{-1} (Fig. 5).

The presence of bands characteristic for both COO^{-} and COOH groups in the spectrum of monomer (Tables 3 and 4) indicates that it represents a mixture of true salt ethacridinium lactate, and a complex between lactic acid and ethacridine, stabilized by hydro-

Table 3
FTIR bands of ethacridine lactate and its oligomers in the wavenumber region 4000–2000 cm^{-1}, and their assignments.

Wavenumbers, cm^{-1}			Assignments[a]
Ethacridine lactate	Oligoethacridine-1	Oligoethacridine-2	
3577 m			ν(O—H)
3421 m			ν_{asym}(N—H) in Ar—NH_2
	3383 m, br	3391 m, br	ν(N—H) in Ar—NH— and —C=NH
3330 m			ν_{sym}(N—H) in Ar—NH_2
3208 s			H-bonded ν(N—H) and $\nu(N^{+}$—H)/overtone of $\delta(NH_2)$
3162 s			H-bonded ν(N—H) and $\nu(N^{+}$—H)
	3106 m	3085 m	H-bonded ν(N—H) and $\nu(N^{+}$—H)
3074 w			H-bonded ν(N—H)/ν(C—H) on Ar ring
3061 w			H-bonded ν(N—H)/ν(C—H) on Ar ring
3014 w-m			ν(C—H) on Ar ring
2987 m			$\nu_{asym}(CH_3)$
2977 m	2977 w	2980 w	$\nu_{asym}(CH_3)$
2936 w	2933 w	2930 w	$\nu_{asym}(CH_2)$
2890 w			$\nu_{sym}(CH_3)$
2872 m			$\nu_{sym}(CH_2)$

Abbreviations: ν – stretching; δ – in-plane bending; s – strong; m – medium; w – weak; br – broad; sym – symmetric; asym – asymmetric; Ar – aromatic.
[a] Assignments based on Refs. [9,44,45].

Table 4
FTIR bands of ethacridine lactate and its oligomers in the wavenumber region 2000–500 cm^{-1}, and their assignments.

Wavenumbers, cm^{-1}			Assignments[a]
Ethacridine lactate	Oligoethacridine-1	Oligoethacridine-2	
1699 m			ν(C═O) in lactate anion
	1664 s, sh	1665 s, sh	ν(C═O) in quinonoid-like structures/ν(C═N)
1647 vs			ν(C═N)/$\delta(NH_2)$ (scissoring) with H-bonding
1632 vs	1625 vs	1623 vs	Acridine and Phz ring-stretching
1607 s		1611 vs	$\delta(NH_2)$ (scissoring)/acridine ring-stretching/Q ring stretching (in N═Q═N) and $\delta_{asym}(NH_3^+)$ in oligomers
1594 s	1592 sh		Acridine ring-stretching
1573 s			$\nu_{asym}(COO^-)$ in lactate anion/Ar ν(C═C)
	1538 m	1538 s	Ring stretching of a new Ar system (Phz-like) in oligomers
1496 vs	1493 s-vs	1495 s	Acridine ring-stretching
1472 sh	1472 s-vs	1470 s	—CH_2— scissoring/acridine ring-stretching
1446 m-s	1442 sh	1442 sh	$\delta_{asym}(CH_3)$/acridine ring-stretching
1415 s			$\nu_{sym}(COO^-)$ in lactate anion
1396 w-m	1396 m	1396 m	—OCH_2 wagging/acridine ring-stretching
1375 m			$\delta_{sym}(CH_3)$
	1363 m	1363 m	Ring stretching of Phz-like units/$\delta_{sym}(CH_3)$
	1350 sh	1350 sh	Acridine ring stretching/ν(C—N) of secondary Ar amine
1341 s			Acridine ring stretching/ν(C—N)/—CH_2— wagging
1314 m	1322 sh	1322 sh	Acridine ring stretching/ν(C—N) of primary or secondary Ar amine
1289 m	1294 w	1293 w	ν(C—N) of primary Ar amine/acridine ring stretching
1268 m			ν(C—N) of primary Ar amine
1254 w	1250 s	1249 s	NH def. vibration of pyridinium salt
1227 vs	1232 vs	1233 vs	ν(═C—O)
	1194 w	1192 w	Ar δ(C—H)
1171 m	1165 w	1164 m	Ar δ(C—H)
1147 m	1146 sh		Ar δ(C—H)
1121 s			Ar δ(C—H)
1114 s	1108 vs	1108 s-vs	ν(O—CH_2)/Ar δ(C—H)/SO_4^{2-}
1099 m			Ar δ(C—H)
	1082 vs	1085 s-vs	SO_4^{2-}/Ar δ(C—H)
1038 s	1037 vs	1036 vs	Stretching of protonated acridine ring/Ar δ(C—H)/$\nu(SO_3)$ in HSO_4^- for oligomers
922 w			ν(C—C)/ν(C—O) in ethoxy group
902 w	898 w	898 w	γ(C—H) 1,2,4-trisubstituted ring (1H)
852 m	853 w, sh	851 w, sh	γ(C—H) 1,2,4-trisubstituted ring (1H)
839 m	836 sh	838 sh	γ(C—H) 1,2,4-trisubstituted ring (2H)
827 m			γ(C—H) 1,2,4-trisubstituted ring (2H), skeletal deformation of substituted acridine
819 m	821 m	822 m	γ(C—H) (1,2,4-trisubstituted ring (2H) for monomer and oligomers and 1,2,3,4-tetrasubstituted ring (2H) for oligomers)
765 m	767 w	767 w	CH_2 rocking/COO^- scissoring
	743 w	743 w	N—H wagging of secondary Ar amine
719			o.p. C═O wag, γ(N—H) of primary Ar amine
657 m	663 w	662 w	γ(OH) in lactate, NH_2 wagging/rocking
	604 m	603 m	HSO_4^- and SO_4^{2-} ions

Abbreviations: ν – stretching; δ – in-plane bending; γ – out-of-plane bending; def. – deformation; vs – very strong; s – strong; m – medium; w – weak; vw – very weak, sh – shoulder; br – broad; i.p. – in-plane; o.p. – out-of-plane; sym – symmetric; asym – asymmetric; Ar – aromatic; Phz – phenazine.

[a] Assignments based on references [9,44,45,47].

gen bonding. The bands of lactate anions are present in the monomer spectrum at 3577 cm^{-1} (sharp band, due to OH stretching), 1573 cm^{-1} (the anti-symmetrical vibration of the COO^- group [45]), and at 1415 cm^{-1} (the symmetrical vibration of the COO^- group [45]), and disappear in the spectra of oligoethacridines (Figs. 4 and 5). The band due to the C═O stretching vibration in COOH group [45], observed at 1699 cm^{-1} in the spectrum of ethacridine lactate, also disappears in the spectra of oligomers. These features clearly evidenced that lactate anions do not serve as counter-ions in the structure of oligoethacridines. On the other side, the presence of SO_4^{2-} and HSO_4^- anions in the structure of oligomers is indicated by the presence of new bands in the spectra of Oligoethacridine-1/Oligoethacridine-2 at 1082/1085 cm^{-1} (broad, assignable to SO_4^{2-} anions) and 604/603 cm^{-1} (attributable to both SO_4^{2-} and HSO_4^- anions), respectively [44]. The band at ~1036 cm^{-1} became relatively much stronger in the spectra of oligomers than in the spectrum of monomer most probably due to the contribution of SO_3 stretching in HSO_4^- anions to the stretching vibration of protonated acridine ring mixed with C—H in-plane bending vibration, δ(C—H). The protonation of the oligomeric samples with H_2SO_4 (salt character of oligoethacridines) is also reflected in the increased absorption above ~1800 cm^{-1} (Figs. 4 and 5).

The presence of two 1,2,4-trisubstituted fused benzene rings in the ethacridine monomer molecule is confirmed by the FTIR bands at 902, 852, 839, 827 and 819 cm^{-1} (Fig. 5, Table 4), due to C—H out-of-plane bending vibrations, γ(C—H) [2a,9,44,45]. The influence of the nature of the substituents (NH_2 and ethoxy group) attached to 1,2,4-trisubstituted benzene rings on the positions of γ(C—H) bands is manifested as appearance of large number of γ(C—H) bands in the region ~900–800 cm^{-1}. In the spectra of oligoethacridines, the strongest band in the "substitution region" is the band at ~821 cm^{-1} (at almost the same position as the band 819 cm^{-1} of monomer), assigned to γ(C—H) vibrations of two adjacent H atoms in remained 1,2,4-trisubstituted rings and newly formed 1,2,3,4-tetrasubstituted rings in oligomers. The bands of monomer at 852 and 839 cm^{-1} are found very weakened (shoulders) at ~853 and 836 cm^{-1}, respectively, in the spectra of oligomers, reflecting the transformation of the 1,2,4-trisubstituted to tetrasubstituted pattern on ethacridine ring during the polymerization process. The change of substitution pattern is also revealed

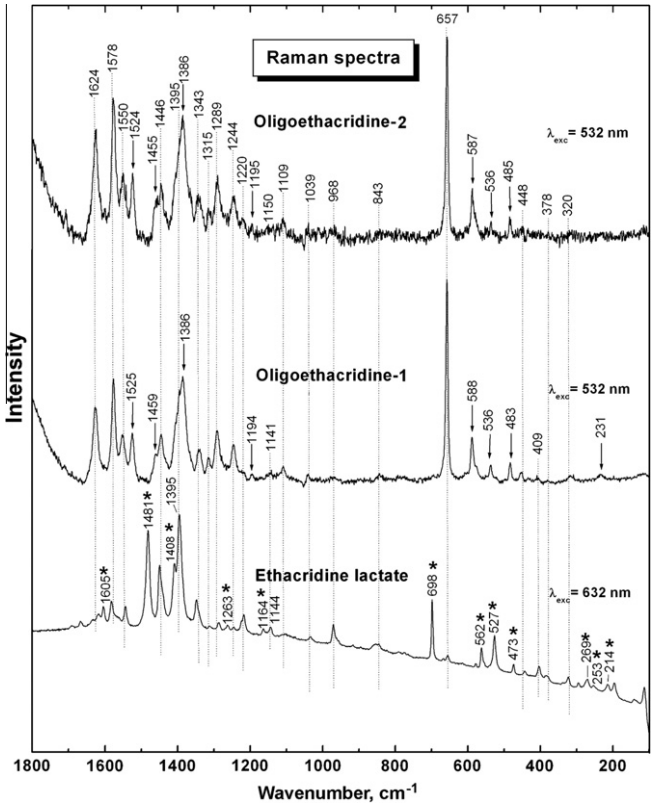

Fig. 6. Raman spectra of ethacridine lactate and oligoethacridine samples in the wavenumber region 1800–100 cm^{-1}; excitation wavelength 633 nm for the monomer and 532 nm for oligomeric samples. The new bands which appeared in the spectra of oligomers in comparison with the spectrum of monomer are marked with an arrow; the bands of monomer which disappeared in the spectra of oligomers are marked with an asterisk.

through the changed positions of bands attributable to δ(C—H) vibrations observed in the spectrum of monomer at 1171, 1147, 1121, and 1099 cm^{-1} and in the spectra of oligoethacridines at ~1194, 1165, and 1146 cm^{-1} (Fig. 5, Table 4).

3.4.3. Raman spectroscopy

The Raman spectra of oligoethacridines were recorded using the excitation wavelength of 532 nm (Fig. 6), because they showed very strong fluorescence when the excitation wavelength of 633 nm has been used. On the other side, more appropriate laser excitation for the Raman spectrum of monomer was 633 nm (Fig. 6).

A new band at ~1525 cm^{-1} in the Raman spectra of oligoethacridines can be assigned to the mixed contribution of N—H bending of secondary amine and C=N stretching of iminoquinonoid segments present in oligoethacridines [1d,48]. Similarly to the FTIR spectra, two Raman bands ascribed to ν(C—N) vibrations of primary aromatic amine are observed in the spectrum of monomer at 1263 and 1286 cm^{-1}, which correspond to stretching vibration of C6—N and C9—N bonds, respectively. In the Raman spectra of oligoethacridines the band at 1263 cm^{-1} completely disappeared due to the participation of C6-bonded NH_2 group in the polymerization reaction, while the presence of a band at 1289 cm^{-1} in the spectra of oligoethacridines indicates that oligomeric chains contain unoxidized NH_2 group bonded to C9 position in ethacridine unit.

New bands observed at 1386 and 588 cm^{-1} in the Raman spectra of oligoethacridines compared with the spectrum of monomer indicate the presence of a new aromatic system, most probably substituted phenazine, in oligomeric chains [48]. In the monomer spectrum, acridine ring-stretching vibration corresponds to the strong peak at 1395 cm^{-1} [47]. The changed substitution pattern on the aromatic rings in oligoethacridines in comparison with that in substituted acridine ring of ethacridine lactate (1,2,4-trisubstitution) is evidenced by the appearance of a new δ(C—H) band at 1194 cm^{-1} in their Raman spectra, and disappearance of δ(C—H) band present in the monomer spectrum at 1164 cm^{-1}. The formation of a new aromatic ring (bearing different substitution pattern) is also indicated by a new peak observed at 1459 and 1455 cm^{-1} in the spectra of Oligoethacridine-1 and Oligoethacridine-2, respectively, ascribed to the aromatic C—C stretching.

The band at ~1244 cm^{-1}, due to the NH deformation vibration characteristic for substituted pyridinium salts [44], is significantly stronger in the spectra of oligoethacridines in comparison with the spectrum of monomer. This spectral feature, which was also observed in the corresponding FTIR spectra (Fig. 5), can be explained by the much more pronounced protonation of fused pyridine ring in oligoethacridine with strong sulfuric acid, formed *in situ* during the oxidative polymerization process, than with weak lactic acid in monomer.

3.4.4. UV–Vis spectroscopy

The UV–Vis spectrum of ethacridine lactate monomer exhibits the absorption bands with maxima at 294, 377, 420, and 435 nm (Fig. 7), the last two maxima being overlapped. In the spectrum of Oligoethacridine-1 the bands with maxima at 291, 353, 414 (shoulder), 430, 484 (shoulder) and 508 nm are observed, and the spectrum of Oligoethacridine-2 exhibits the bands with maxima at 311, 353, 430, and 509 nm. The appearance of new bands in the spectra of oligomers related to the spectrum of monomer, i.e. the band with overlapping maxima at 508 and 484 nm in the spectrum of Oligoethacridine-1, and the band at 509 nm for Oligoethacridine-2, reflects the presence of more extended conjugated system in oligomers in comparison with that of the monomer. These new bands may also be attributed to the oxidized oligomeric structures, which contain non-cyclized ortho-iminoquinonoid (quinonediimine-like) (structure **6**, Scheme 3), dihydrophenazine-like (structure **7**, Scheme 3) and/or phenazine-like (structure **8**, Scheme 3) units. The spectra of both oligoethacridine samples show the band at 430 nm (with the shoulder at ~414 nm in the spectrum of Oligoethacridine-1). Since this absorption maximum wavelength is close to the wavelength of the maxima at 420/435 nm in the spectrum of monomer, it can be supposed that the band at 430 nm reflects the presence of reduced acridine-type units (similar to original monomeric unit) in the oligomers (structure **5**, Scheme 3), and the presence of lower oligomers (dimers, trimers). The band at close position (~400–460 nm) has been frequently found in the UV–Vis spectra of polymers of aromatic diamines which contain phenazine-type units, and has been attributed to a $\pi \rightarrow \pi^*$ transition associated with phenazine unit conjugated to the lone pairs of bridging nitrogens [12].

3.4.5. EPR spectroscopy

EPR spectroscopy reveals the existence of paramagnetic (cation radical) segments in oligoethacridines, Fig. 8. Based on elemental analysis and FTIR, Raman and EPR spectroscopy, it can be concluded that the oxidation of ethacridine lactate with peroxydisulfate in the aqueous solution of hydrochloric acid leads to the formation of $N_{(C6)}$–C5 coupled oligoethacridines, which contain both reduced (aminobenzenoid) and oxidized (paramagnetic semiquinonoid, diamagnetic quinonoid, substituted phenazine) segments (Scheme 4). Precipitated oligoethacridines contain sulfate/hydrogen sulfate and chloride anions as counter ions of the positively charged oligomeric chains. The experimental findings are in excellent agreement with computational predictions of the molecular structure of prevalent ethacridine dimer units.

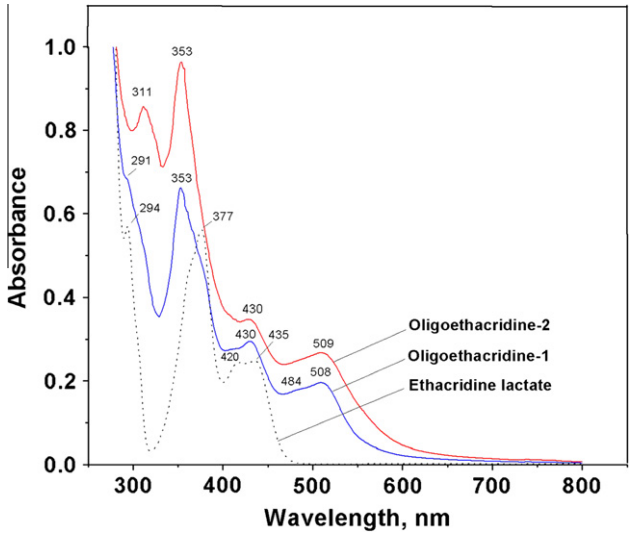

Fig. 7. UV–Vis spectra of ethacridine lactate and oligoethacridine samples dissolved in DMSO.

3.5. Electroactivity of oligoethacridines

Cyclic voltammetry confirmed that both oligoethacridine samples are electroactive (Fig. 9), redox behavior of Oligoethacridine-1 being more complex. Electroactivity of Oligoethacridine-1 is expressed by two redox couples, O_1/R_1 and O_2/R_2 (Fig. 9 top), while Oligoethacridine-2 shows one redox couple, O_1/R_1 (Fig. 9 bottom). It can be seen that the redox couple O_1/R_1, observable between −0.3 and +0.1 V vs. SCE, is present for both samples. Apparently, reduction takes place as a two-step process (peaks R_1' and R_1''), while only one corresponding oxidation peak (O_1) appears upon the inversion of polarization. Shifting of the peak potential with polarization rate reveals an irreversible behavior. Another redox couple O_2/R_2, located in the potential window between +0.4 and +0.7 V vs. SCE, is characteristic only for Oligoethacridine-1. Peak separation and the dependence of the peak potential on the rate of polarization designate irreversible behavior in this case, too. Redox couple denoted as B_O/B_R was observed in free solution (supporting electrolyte) and will not be discussed here. Upon deep anodic polarization (E > +1.0 V vs. SCE) extensive oxidation of oligoethacridines is observed, being more pronounced in the case of Oligoethacridine-1. No corresponding cathodic peak is recorded in this case, indicating irreversible formation of oxidation products, or rapid chemical transformation of electrochemically formed oxidation products of oligoethacridine lactate.

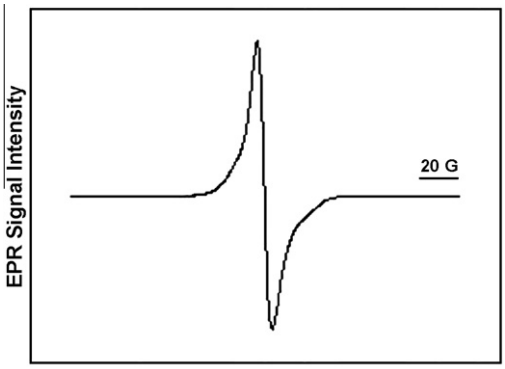

Fig. 8. EPR spectrum of Oligoethacridine-1.

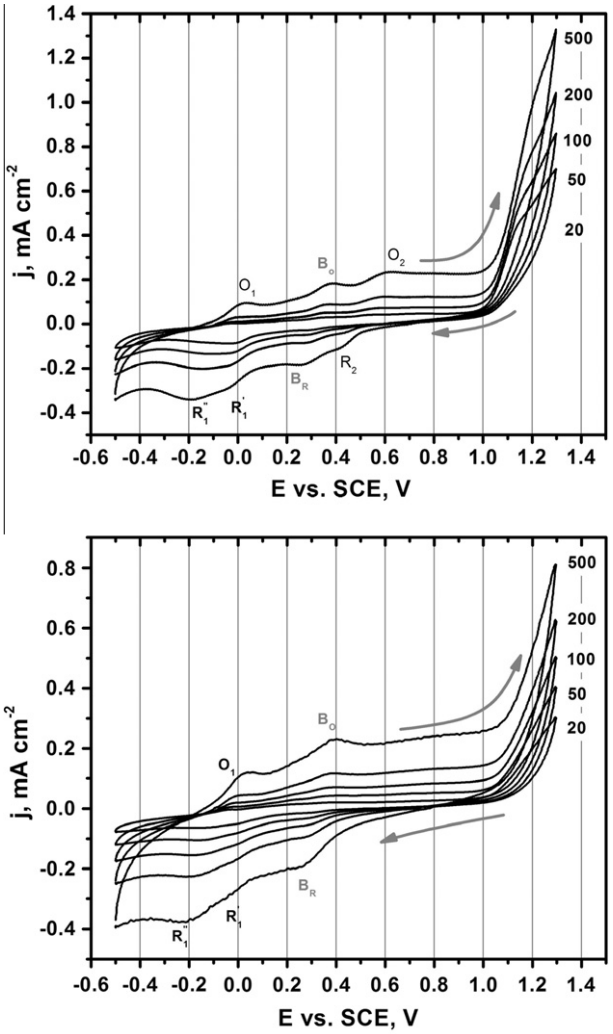

Fig. 9. Cyclic voltammograms of the oxidation products of ethacridine lactate, Oligoethacridine-1 (top) and Oligoethacridine-2 (bottom), recorded in DMSO + 0.2 M·H_2SO_4 solution at GC electrode with different polarization rates in the range from 20 to 500 mV/s as indicated on the figures.

4. Conclusions

Ethacridine oligomers, with the weight-average molecular weight M_w = 1980 and 1930 and the number-average molecular weight M_n = 1630 and 1560, were synthesized for the first time by the oxidation of the ethacridine lactate with ammonium peroxydisulfate at oxidant-to-monomer mole ratios 1.25 and 2.5, respectively, in a hydrochloric acid aqueous solution at room temperature. MALDI-TOF MS evidenced the presence of oligomeric species from dimers up to hexamers; the signal decreased with increase of molecular weight. Oligoethacridines protonated by both hydrochloric acid and *in situ* formed sulfuric acid, as revealed by the elemental analysis, are nonconducting ($\sim 6.5 \times 10^{-9}$ S cm^{-1}) and have fragmental and submicro/micro-layered morphology. Molecular orbital RM1 computations, combined with the MM2 molecular mechanics force-field method and conductor-like screening model of solvation, indicate that oligoethacridines contain $N_{(C6)}$–C5 coupled diethacridine unit as the major structural segment which can exist in both reduced (aminobenzenoid) and oxidized (iminoquinonoid) form. Quantum chemical prediction of ethacridine oligomerization pathway is consistent with the results from FTIR spectroscopic analysis, which confirmed the oxidative transformation of $NH_{2(C6)}$ group of monomer. The formation of

oligomers, as well as the presence of both reduced and oxidized structural units in the oligomers was proved by the UV–Vis spectroscopy. FTIR and Raman spectroscopies also proved the presence of phenazine-like units in ethacridine oligomers. Paramagnetism, caused by the existence of cation radical diethacridine structural segments, and electroactivity of the oligoethacridines were proved by EPR and cyclic voltammetry, respectively.

Acknowledgements

The authors thank the Ministry of Education and Science of Serbia (Contracts 172035 and 172043, and HPSEE European project) and Czech Grant Agency (203/08/0686) for financial support.

References

[1] (a) R.H. Sestrem, D.C. Ferreira, R. Landers, M.L.A. Temperini, G.M. do Nascimento, Eur. Polym. J. 46 (2010) 484–493;
(b) G. Zhang, A. Zhang, X. Liu, S. Zhao, J. Zhang, J. Lu, J. Appl. Polym. Sci. 115 (2010) 2635–2647;
(c) S.M. Sayyah, S.S. Abd El-Rehim, M.M. El-Deeb, S.M. Kamal, R.E. Azooz, J. Appl. Polym. Sci. 117 (2010) 943–952;
(d) R.H. Sestrem, D.C. Ferreira, R. Landers, M.L.A. Temperini, G.M. do Nascimento, Polymer 50 (2009) 6043–6048;
(e) M. Hébert, D. Rochefort, Electrochim. Acta 53 (2008) 5272–5279;
(f) X.-G. Li, X.-L. Ma, J. Sun, M.-R. Huang, Langmuir 25 (2009) 1675–1684.
[2] (a) G. Ćirić-Marjanović, M. Trchová, E.N. Konyushenko, P. Holler, J. Stejskal, J. Phys. Chem. B 112 (2008) 6976–6987;
(b) Q. Sun, Y. Deng, Eur. Polym. J. 44 (2008) 3402–3408;
(c) M.A. Cotarelo, F. Huerta, C. Quijada, R. Mallavia, J.L. Vázquez, J. Electrochem. Soc. 153 (2006) D114–D122.
[3] (a) M.A. Rahman, M.-S. Won, N.-H. Kwon, J.-H. Yoon, D.-S. Park, Y.-B. Shim, Anal. Chem. 80 (2008) 5307–5311;
(b) M.-S. Won, J.-H. Yoon, Y.-B. Shim, Electroanalysis 17 (2005) 1952–1958;
(c) M. Tagowska, B. Pałys, M. Mazur, M. Skompska, K. Jackowska, Electrochim. Acta 50 (2005) 2363–2370;
(d) A. Nasalska, M. Skompska, J. Appl. Electrochem. 33 (2003) 113–119;
(e) S.-Y. Honga, S.-M. Park, J. Electrochem. Soc. 150 (2003) E360–365.
[4] (a) M. Gao, F. Yang, G. Zhang, L. Liu, X. Wang, Electrochim. Acta 54 (2009) 2224–2228;
(b) F. Yakuphanoglu, B.F. Şenkal, Synth. Met. 159 (2009) 311–314;
(c) F. Yakuphanoglu, B.F. Senkal, Polym. Adv. Technol. 19 (2008) 1193–1198;
(d) M. Gao, F. Yang, X. Wang, G. Zhang, L. Liu, J. Phys. Chem. C 111 (2007) 17268–17274;
(e) X.G. Li, H. Li, M.R. Huang, Chem. Eur. J. 13 (2007) 8884–8896.
[5] (a) G.M. do Nascimento, V.R.L. Constantino, M.L.A. Temperini, J. Phys. Chem. B 108 (2004) 5564–5571;
(b) G.M. do Nascimento, P.S.M. Barbosa, V.R.L. Constantino, M.L.A. Temperini, Colloids Surf. A 289 (2006) 39–46.
[6] G. Ćirić-Marjanović, B. Marjanović, M. Trchová, P. Holler, Mater. Sci. Forum 494 (2005) 357–362.
[7] F. D'Eramo, M.A. Zón, H. Fernández, L. Sereno, A.H. Arévalo, Electrochim. Acta 53 (2008) 7182–7190.
[8] (a) F. Bakhtiarzadeh, S. Ab Ghani, Electroanalysis 22 (2010) 549–555;
(b) B. Shentu, K. Oyaizub, H. Nishide, J. Mater. Chem. 14 (2004) 3308–3311.
[9] G. Ćirić-Marjanović, N.V. Blinova, M. Trchová, J. Stejskal, J. Phys. Chem. B 111 (2007) 2188–2199.
[10] B. Marjanović, G. Ćirić-Marjanović, A. Radulović, I. Juranić, P. Holler, Mater. Sci. Forum 555 (2007) 503–508.
[11] M. Skompska, M. Chmielewski, A. Tarajko, Electrochem. Commun. 9 (2007) 540–544.
[12] X.-G. Li, M.-R. Huang, W. Duan, Y.-L. Yang, Chem. Rev. 102 (2002) 2925–3030.
[13] G. Pierre, M. Abdel-Azzem, U.S. Yousef, Eur. Polym. J. 34 (1998) 819–826.
[14] (a) S.J. Killoran, R.D. O'Neill, Electrochim. Acta 53 (2008) 7303;
(b) L.J. Murphy, Anal. Chem. 70 (1998) 2928–2935.
[15] J. Yano, S. Yamasaki, Synth. Met. 102 (1999) 1157.
[16] K. Ogura, H. Shiigi, M. Nakayama, J. Electrochem. Soc. 143 (1996) 2925–2930.
[17] A. Puzari, J.B. Baruah, React. Funct. Polym. 47 (2001) 147–152.
[18] V.N. Popok, I.A. Karpovich, V.B. Odzhaev, D.V. Sviridov, Nucl. Instrum. Meth. Phys. Res. B 148 (1999) 1106–1110.
[19] (a) A.A. Abdelwahab, H.-M. Lee, Y.-B. Shim, Anal. Chim. Acta 650 (2009) 247–253;
(b) J.C. Vidal, E. Garcia-Ruiz, J. Espuelas, T. Aramendia, J.R. Castillo, Anal. Bioanal. Chem. 377 (2003) 273–280.
[20] Q. Xu, C. Xu, Y. Wang, W. Zhang, L. Jin, K. Tanaka, H. Haraguchi, A. Itoh, Analyst 125 (2000) 1453–1457.
[21] (a) R. Ojani, J.B. Raoof, S.R.H. Zavvarmahalleh, J. Solid State Electrochem. 13 (2009) 1605–1611;
(b) M.H. Pournaghi-Azar, B. Habibi, J. Electroanal. Chem. 601 (2007) 53–62.
[22] (a) J.-J. Wang, J. Jiang, B. Hu, S.-H. Yu, Adv. Funct. Mater. 18 (2008) 1105;
(b) K. Kilian, K. Pyrzynska, React. Funct. Polym. 68 (2008) 974–980;
(c) M.-R. Huang, Q.-Y. Peng, X.-G. Li, Chem. Eur. J. 12 (2006) 4341–4350;
(d) X.-G. Li, M.-R. Huang, S.-X. Li, Acta Mater. 52 (2004) 5363–5374;
(e) M. Skompska, A.R. Hillman, J. Chem. Soc. Faraday Trans. 92 (1996) 4101–4108.
[23] L.F. D'Elia, R.L. Ortíz, O.P. Marquez, J. Márquez, Y. Martínez, J. Electrochem. Soc. 148 (2001) C297–300.
[24] A. Meneguzzi, M.C. Pham, J.C. Lacroix, B. Piro, A. Adenier, C.A. Ferreira, P.C. Lacaze, J. Electrochem. Soc. 148 (2001) B121–B126.
[25] (a) S.A. Hashmi, S. Suematsu, K. Naoi, J. Power Sources 137 (2004) 145–151;
(b) K. Naoi, S. Suematsu, A. Manago, J. Electrochem. Soc. 147 (2000) 420–426.
[26] Martindale – The complete drug reference, thirty sixth ed., Pharmaceutical Press, 2009, p. 1625.
[27] J.-J. Xu, H.-Y. Chen, Anal. Chim. Acta 423 (2000) 101–106.
[28] (a) M.J.S. Dewar, E.G. Zoebisch, E.F. Healy, J.J.P. Stewart, J. Am. Chem. Soc. 107 (1985) 3902–3909;
(b) J.J.P. Stewart, J. Comput. Chem. 10 (1989) 209–220.
[29] J.J.P. Stewart, J. Comput. Aid. Mol. Des. 4 (1990) 1–103.
[30] G.B. Rocha, R.O. Freire, A.M. Simas, J.J. P Stewart, J. Comp. Chem. 27 (2006) 1101–1111.
[31] L.Y. Dávila, M.J. Caldas, J. Comp. Chem. 23 (2002) 1135–1142.
[32] A. Klamt, G. Schüürmann, J. Chem. Soc. Perk. Trans. 2 (1993) 799–805.
[33] U. Burkert, N.L. Allinger, Molecular Mechanics, American Chemical Society, Washington, DC, 1982.
[34] A. Banerjee, N. Adams, J. Simons, R. Shepard, J. Phys. Chem. 89 (1985) 52–57.
[35] J. Baker, J. Comp. Chem. 7 (1986) 385–395.
[36] M. Netopilík, P. Kratochvíl, Polymer 44 (2003) 3431–3436.
[37] J. Horský, Polym. Commun. 32 (1991) 346–347.
[38] (a) M.-R. Huang, S.-J. Huang, X.-G. Li, J. Phys. Chem. C 115 (2011) 5301–5315;
(b) X.-G. Li, Y.-W. Liu, M.-R. Huang, S. Peng, L.-Z. Gong, M.G. Moloney, Chem. Eur. J. 16 (2010) 4803–4813.
[39] H. Pasch, W. Schrepp, MALDI-TOF Mass Spectrometry of Synthetic Polymers, Springer, Berlin Heidelberg, 2003.
[40] G. Ćirić-Marjanović, M. Trchová, J. Stejskal, Collect. Czech. Chem. Commun. 71 (2006) 1407–1426.
[41] G. Ćirić-Marjanović, M. Trchová, J. Stejskal, Int. J. Quantum Chem. 108 (2008) 318–333.
[42] G. Ćirić-Marjanović, E.N. Konyushenko, M. Trchová, J. Stejskal, Synth. Met. 158 (2008) 200–211.
[43] G.S. Hammond, J. Am. Chem. Soc. 77 (1955) 334–338.
[44] G. Socrates, Infrared and Raman Characteristic Group Frequencies, John Wiley & Sons, New York, 2001. pp. 102, 103, 108, 109, 129, 157–167, 169, 171, 173, 285, 290, 291.
[45] L.J. Bellamy, The Infra-red Spectra of Complex Molecules, Richard Clay, Bungay, Suffolk, 1962. pp. 139, 140, 150, 226–229, 233–239, 284.
[46] D.L. Vien, N.B. Colthup, W.G. Fateley, J.G. Grasselli, The Handbook of Infrared and Raman Characteristic Frequencies of Organic Molecules, Academic Press, San Diego, 1991.
[47] M.B. Mitchell, G.R. Smith, W.A. Guillory, J. Chem. Phys. 75 (1981) 44–48.
[48] G. Ćirić-Marjanović, M. Trchová, J. Stejskal, J. Raman Spectrosc. 39 (2008) 1375–1387.